

Detection accuracy of target accelerations based on vortex electromagnetic wave in keyhole space

Kai Guo(郭凯), Shuang Lei(雷爽), Yi Lei(雷艺), Hong-Ping Zhou(周红平), and Zhong-Yi Guo(郭忠义)
Citation: Chin. Phys. B, 2024, 33 (**2**): 020603. DOI: 10.1088/1674-1056/ad071a
Journal homepage: http://cpb.iphy.ac.cn; http://iopscience.iop.org/cpb

What follows is a list of articles you may be interested in

Structure study of a dielectric laser accelerator with discrete translational symmetry

Yangfan He(何阳帆), Bin Sun(孙斌), Mingjiang Ma(马铭江), Wei Li(李伟), Zhihao Cui(崔志浩), and Zongqing Zhao(赵宗清)
Chin. Phys. B, 2023, 32 (**11**): 114101. DOI: 10.1088/1674-1056/acc05a

Quantum estimation of rotational speed in optomechanics

Hao Li(李浩) and Jiong Cheng(程泂)
Chin. Phys. B, 2023, 32 (**10**): 100602. DOI: 10.1088/1674-1056/ace3b7

Design, fabrication and optimization of electromagnetic absorption metamaterials

Qi Lou(娄琦), Xu-Dong Zhang(张旭东), and Ming-Gang Xia(夏明岗)
Chin. Phys. B, 2023, 32 (**9**): 094102. DOI: 10.1088/1674-1056/accb42

Design of an optically-transparent ultra-broadband microwave absorber

Mian Gao(高冕), Qiang Chen(陈强), Yue-Jun Zheng(郑月军), Fang Yuan(袁方), Zhan-Shan Sun(孙占山), and Yun-Qi Fu(付云起)
Chin. Phys. B, 2023, 32 (**8**): 084102. DOI: 10.1088/1674-1056/ac9a39

Signal-recycled weak measurement for ultrasensitive velocity estimation

Sen-Zhi Fang(方森智), Yang Dai(戴阳), Qian-Wen Jiang(姜倩文), Hua-Tang Tan(谭华堂), Gao-Xiang Li(李高翔), and Qing-Lin Wu(吴青林)
Chin. Phys. B, 2021, 30 (**6**): 060601. DOI: 10.1088/1674-1056/abda2d

---

Detection accuracy of target accelerations based on vortex electromagnetic wave in keyhole space

Kai Guo(郭凯)[†], Shuang Lei(雷爽), Yi Lei(雷艺), Hong-Ping Zhou(周红平), and Zhong-Yi Guo(郭忠义)

School of Computer and Information, Hefei University of Technology, Hefei 230009, *China*

(Received 14 September 2023; revised manuscript received 20 October 2023; accepted manuscript online 26 October 2023)

The influence of the longitudinal acceleration and the angular acceleration of detecting target based on vortex electromagnetic waves in keyhole space are analyzed. The spectrum spreads of different orbital angular momentum (OAM) modes in different non-line-of-sight situations are simulated. The errors of target accelerations in detection are calculated and compared based on the OAM spectra spreading by using two combinations of composite OAM modes in the keyhole space. According to the research, the effects about spectrum spreads of higher OAM modes are more obvious. The error in detection is mainly affected by OAM spectrum spreading, which can be reduced by reasonably using different combinations of OAM modes in different practical situations. The above results provide a reference idea for investigating keyhole effect when vortex electromagnetic wave is used to detect accelerations.

Keywords: vortex electromagnetic waves, detect accelerations, keyhole space, spectrum spread

PACS: 06.30.Gv, 41.20.Jb **DOI:** 10.1088/1674-1056/ad071a

1. Introduction

Electromagnetic wave can carry not only spin angular momentum (SAM) but also orbital angular momentum (OAM),[1,2] which are related to circular polarization and helical phase structure. Electromagnetic wave carrying OAM is called as vortex wave[3] and shows huge advantages over conventional electromagnetic wave in practical application owing to its unique features. The orthogonality between different OAM modes provides extra degrees of freedom in addition to conventional physical components of electromagnetic wave, increasing the capacity of communication channel[4,5] and improving the resolution of imaging.[6–8] In addition, the coupling between OAM of electromagnetic wave and mechanical momentum has been utilized to manipulate particles.[9] In recent years, the rotational Doppler effect of vortex electromagnetic wave has offered a simple method to obtain three-dimensional information of a moving object, such as velocity and acceleration.[10–12] So far, there have been extensive researches on vortex electromagnetic wave, including generation of high-quality OAM modes,[13,14] efficient detection method,[15] and its propagation characteristic through inhomogeneous medium.[16]

Practically, environment has great influence on the transmission of electromagnetic vortex beams, causing crosstalk among OAM modes. In 2005, the concept of OAM spectrum was proposed in optics.[17] Subsequently, the OAM spectrum characteristics of vortex beams were extensively studied over a broadband electromagnetic spectrum in different transmission environments. On the one hand, the OAM spectrum spreading of optical beams has been carefully studied after passing through atmosphere[18,19] and seawater turbulences.[20,21] On the other hand, in the radio frequency range, the transmission of vortex electromagnetic wave is more obviously affected by the scattering of obstacles.[22–24] The scattering of high-order Bessel vortex electromagnetic waves on dielectric spheres was studied.[22] Fortunately, the OAM spectrum maintains well after the vortex electromagnetic wave has transmitted through conductor sphere and cone.[23] Very recently, it was reported that the off-axis vortex waves illuminate electrically large conductors of different shapes.[24]

These results indicate that the OAM spectrum spreading due to inhomogeneous transmission environment will inevitably bring negative influence on the application of vortex beam. However, as a unique feature of vortex electromagnetic wave, the rotating Doppler effect and its application in detecting a rotating target have been studied mostly within the ideal line-of-sight scenarios until now.[25–30] Especially, the OAM spectrum spreading caused by non-line-of-sight scenario and non-cooperative target simultaneously is difficult to predict directly.[12] Therefore, it is urgent in practice to study the detection of rotating targets in non-line-of-sight scenarios. A "keyhole space" model for a typical non-line-of-sight scenario has been investigated in communication system with vortex electromagnetic wave.[31–33] For example, for indoor users to detect outdoor targets, the opacity of the wall to the signal will cause energy to leak out only through windows, doors, and other keyholes. Even in outdoor scenarios with abundant scattering environment, the keyhole effect can occur when the ring of the scattering object is smaller than the distance between the transmitter and the receiver.[34] However, the performance of detecting rotating targets with vortex electromagnetic wave

[†]Corresponding author. E-mail: kai.guo@hfut.edu.cn

© 2024 Chinese Physical Society and IOP Publishing Ltd

still remains to be studied in the keyhole space model.

In this work, we use the vortex electromagnetic wave in the keyhole space to detect a rotating target. The rest of this paper is organized as follows. In Section 2 the detection principle and analysis method are described. In Section 3 are studied the OAM spectrum spreading of vortex electromagnetic wave in several typical keyhole space situations. In Section 4, the detection errors of both longitudinal and angular accelerations of the target are calculated and analyzed. Finally, some conclusions are drawn from the present study in Section 5.

2. Detection principle and analysis method

Figure 1 schematically shows the detection of the rotating target by using the model of vortex electromagnetic wave in the keyhole space. The vortex electromagnetic wave is generated by an eight-arm Archimedes spiral antenna (ASA)[35] with a radius of 150 mm, propagates along the z axis, and encounters the keyhole space that is symmetric about the z axis 450 mm away. Considering the common diffraction aperture, a circular keyhole with radius R is studied and its surrounding material is set as a perfect electric conductor (PEC).[33] After passing through the keyhole space, the vortex electromagnetic wave with spread OAM spectrum reaches the target 900 mm away, which rotates perpendicular to the z axis with angular velocity $\Omega_0 + g't$ and moves along the z axis with longitudinal velocity $v_0 + gt$. Ω_0 and v_0 are the initial angular velocity and longitudinal velocity, respectively, g' and g are the angular acceleration and longitudinal acceleration, respectively. In the variable acceleration case, the longitudinal variable acceleration of the target is $g(t) = g_0 + pt$, and the angular variable acceleration is $g'(t) = g'_0 + p't$, with p and p' being longitudinal variable acceleration and angular variable acceleration, respectively. Without loss of generality, the target can be treated as a scattering point in the far field.

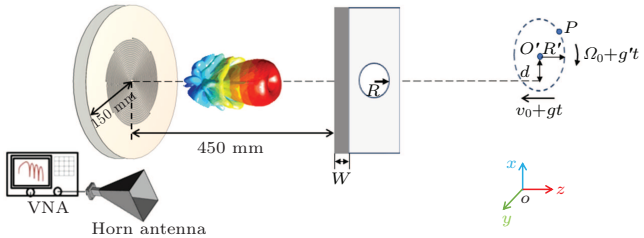


Fig. 1. Detection model of longitudinally and angularly accelerated target with vortex electromagnetic wave in keyhole space.

In a line-of-sight scenario, the signal received by antenna can be expressed as[12]

$$
\begin{aligned}
E_{\mathrm{r}}(t) &= \mathrm{e}^{\mathrm{i}2\pi f_{\mathrm{c}}[t-2(r-s(t))/c]}\frac{\mathrm{e}^{-\mathrm{i}2kr}}{r^2}\mathrm{e}^{\mathrm{i}l(\varphi_0+\varphi(t))}J_l(ka\sin\theta)\,\sigma,\\
s(t) &= \int_{t_0}^{t} v(t)\,\mathrm{d}t = \int_{t_0}^{t}(v_0+gt)\,\mathrm{d}t,\\
\varphi(t) &= \int_{t_0}^{t}\Omega(t)\,\mathrm{d}t = \int_{t_0}^{t}(\Omega_0+g't)\,\mathrm{d}t,
\end{aligned}
\tag{1}
$$

where f_{c} is the carrier frequency, k is the wave number, r is the distance between the antenna and the target, $s(t)$ is the relative distance difference, $\varphi(t)$ is the relative azimuth difference, σ is the scattering coefficient, φ_0 is the initial azimuth, and a is the antenna radius.

Based on Eq. (1) and time-frequency analysis method. we use a commonly used time-frequency analysis method to analyze time-varying non-stationary signals. It has an exponential kernel function, which can effectively suppress the interference term and maintain a high time-frequency resolution.[12] The slope of the time-frequency signal could be expressed as

$$
m = \frac{\mathrm{d}\Delta f(t)}{\mathrm{d}t} = \frac{2f_{\mathrm{c}}g}{c} + \frac{g'l}{2\pi}, \tag{2a}
$$

$$
m = \frac{\mathrm{d}^2\Delta f(t)}{\mathrm{d}t^2} = \frac{f_{\mathrm{c}}p}{c} + \frac{p'l}{4\pi}, \tag{2b}
$$

where the first part (Eq. (2a)) and second part (Eq. (2b)) correspond to uniform acceleration and variable acceleration, respectively, $\Delta f(t)$ is the Doppler frequency shift, g and g' are the longitudinal and angular uniform acceleration, respectively, p and p' are the longitudinal variable acceleration and angular variable acceleration, respectively, and the value of m could be estimated by fitting method. When transmitting signals of different OAM modes with topological charges of l_1 and l_2 simultaneously, the angular uniform acceleration (AUA), longitudinal uniform acceleration (LUA), the angular variable acceleration (AVA) and longitudinal variable acceleration (LVA) of target can be expressed as

$$
\begin{aligned}
g' &= \frac{2\pi(m_2-m_1)}{l_2-l_1}, \quad g = \frac{(2\pi m - g'l)\,c}{4\pi f_{\mathrm{c}}},\\
p' &= \frac{4\pi(m_2-m_1)}{l_2-l_1}, \quad p = \frac{(4\pi m - p'l)\,c}{4\pi f_{\mathrm{c}}}.
\end{aligned}
\tag{3}
$$

However, in keyhole space, OAM beam is blocked and does not fully illuminate the object, which results in the spread of OAM spectrum. Therefore, the transmitting signal when reaching the target can be expressed as

$$
\begin{aligned}
E_t(t) &= \sum_{-\infty}^{\infty} A_l\,\mathrm{e}^{\mathrm{i}2\pi f_{\mathrm{c}}t}\frac{\mathrm{e}^{-\mathrm{i}kr}}{r^2}\mathrm{e}^{\mathrm{i}l\varphi_0}J_l(ka\sin\theta),\\
A_l &= \frac{1}{2\pi}\int_0^{2\pi} E(\varphi)\,\mathrm{e}^{-\mathrm{i}l\varphi}\,\mathrm{d}\varphi,
\end{aligned}
\tag{4}
$$

where A_l is the weight of the OAM mode with the topological charge l.

Without considering the attenuation of the transmission path, the frequency shift information carried by the moving target in the echo signal is only time-dependent. When the phase is differentiated with respect to time, all the phase effects independent of time are eliminated. Therefore, the slope

of the time-frequency signal for the uniform acceleration can be expressed as

$$m' = \begin{cases} \dfrac{2f_c g}{c} + \dfrac{g' l_1}{2\pi}, \\ \dfrac{2f_c g}{c} + \dfrac{g' l_2}{2\pi}, \\ \cdots, \\ \dfrac{2f_c g}{c} + \dfrac{g' l_k}{2\pi}, \end{cases} \tag{5}$$

and the slope of the time-frequency signal for the variable acceleration be expressed as

$$m' = \begin{cases} \dfrac{f_c p}{c} + \dfrac{p' l_1}{4\pi}, \\ \dfrac{f_c p}{c} + \dfrac{p' l_2}{4\pi}, \\ \cdots, \\ \dfrac{f_c p}{c} + \dfrac{p' l_k}{4\pi}. \end{cases} \tag{6}$$

We obtain the slope m' that can be expressed by using data fitting that is affected by different values of m. The AUA, LUA, AVA, and LVA of target can be expressed as

$$\begin{aligned} g_1' &= \frac{2\pi\,(m_2' - m_1')}{l_2 - l_1}, \quad g_1 = \frac{(2\pi m' - g' l)\,c}{4\pi f_c}, \\ p_1' &= \frac{4\pi (m_2' - m_1')}{l_2 - l_1}, \quad p_1 = \frac{(4\pi m' - p' l)\,c}{4\pi f_c}. \end{aligned} \tag{7}$$

The errors can be calculated as

$$\text{error} = \begin{cases} \dfrac{g_1' - g'}{g'} \times 100\%, & \dfrac{p_1' - p'}{p'} \times 100\%, \\ \dfrac{g_1 - g}{g} \times 100\%, & \dfrac{p_1 - p}{p} \times 100\%. \end{cases} \tag{8}$$

Both the keyhole space and the attitude of the target will lead to the impurities of the OAM modes and increased errors in detection of angular and longitudinal accelerations. We will study these issues in detail in future work.

3. Results and discussion

3.1. OAM spectra spreading

Without loss of generality, the OAM spectrum spreading of vortex electromagnetic wave with the topological charge of $l = 1$ and $l = 2$ at $f = 2.45$ GHz are analyzed under different keyhole conditions by numerical simulation. In an actual detection, we only need to predict the error range of the acceleration and do not need to obtain a specific spectrum spread. However, in order to analyze the source of the errors, we measure the OAM spectrum spreading of vortex electromagnetic wave by using a uniform circular antenna (UCA) array with 256 sampling points.[15]

Firstly, we investigate the keyhole spaces with different radii of $R = 0.5\lambda$, $R = 0.7\lambda$, $R = \lambda$, $R = 1.5\lambda$. Besides, two other cases are studied: one is the keyhole radius equal to that of the transmitting antenna ASA (r of ASA), and the other is the free space. The thickness of the keyhole is 5 mm[33] and the radius of circular observation surface is 85 mm, which is equal to the radius of the radiating area of the transmitting antenna ASA.

Figures 2(a) and 2(b) show the mode purities of OAM beams with topological charge of $l = 1$ and $l = 2$, respectively, after passing the keyhole spaces with different radii. The purities of main modes become higher when the radius of keyhole increases, because the influence of diffraction at the keyhole on the spiral phase construction of OAM beams becomes less. However, figure 2(b) shows that the OAM spectra spreading is more obvious for the case with $l = 2$. It is because the energy of the OAM beams mainly concentrates into a 'donut', most of energy locates at a ring with radius of 90 mm and 170 mm for the case with $l = 1$ and $l = 2$, respectively, at the keyhole space. Therefore, the destruction of spiral phase is more serious with $l = 2$ for the same radius of keyhole.

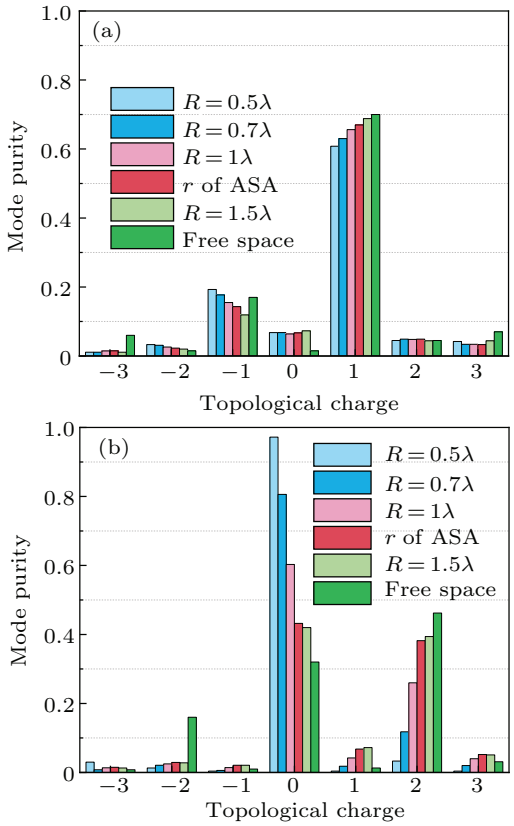


Fig. 2. OAM spectra of vortex electromagnetic waves with topological charge of $l = 1$ (a) and $l = 2$ (b), exiting from Archimedes spiral antenna and after passing a keyhole space with different radii.

Secondly, the thickness of the keyhole is investigated, and the value of w is set to 5 mm, 30 mm, 60 mm, 100 mm, and 200 mm in simulation. Without loss of generality, the radius of keyhole is set as λ and the radius of circular observation surface is 85 mm.

Figures 3(a) and 3(b) show the mode purities of OAM beam with $l = 1$ and $l = 2$, respectively, after passing the keyhole space with different thicknesses. The OAM beam with

$l = 1$ can pass through the keyhole completely due to the small size of its energy 'donut'. Therefore, the OAM spectrum spreading is not obvious with $l = 1$ as the thickness increases. For the OAM beam with $l = 2$, the range of energy can exceed the size of keyhole, fortunately, the divergence of OAM beam will be limited during propagation in the keyhole space, resulting in a focusing effect. Therefore, the purity of main mode is improved more obviously with $l = 2$.

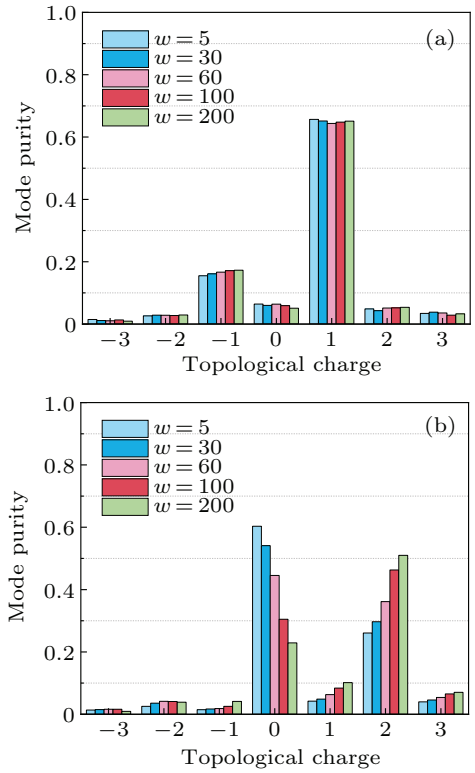


Fig. 3. OAM spectra of vortex electromagnetic wave with $l = 1$ (a) and $l = 2$ (b) after passing keyhole with different thicknesses.

Thirdly, it is considered that the attitude of the target may exert an influence on OAM mode in the keyhole space. As shown in Fig. 1, the target is moving along the UCA array. The radius of keyhole is set as λ and its thickness is 5 mm, and different radii of target trajectory are investigated: $R' = 85$ mm, 105 mm, 150 mm, 250 mm, and 400 mm.

Figures 4(a) and 4(b) show the mode purities of OAM beam with $l = 1$ and $l = 2$, respectively, in the case of different radii of the target trajectories. It can be seen that the purity of the main mode with $l = 1$ first increases and then decreases gradually, while the purity of main mode with $l = 2$ is improved obviously. Because most of energy is located at a ring with radius of 130 mm and 300 mm for the case with $l = 1$ and $l = 2$, respectively, at the observation surface. If the target rotates at the ring where the OAM beam has the strongest energy, the purity of the main mode is the best.

Finally, the centers of the target at different off-axis distances are investigated. As shown in Fig. 1, its centers are located at (0, d, 900 mm), where d indicates the off-axis distance. In simulation, the value of d is set to 0, 100 mm, 200 mm, 300 mm, and 400 mm. The thickness of the keyhole is 5 mm and the radius of circular observation surface is 85 mm.

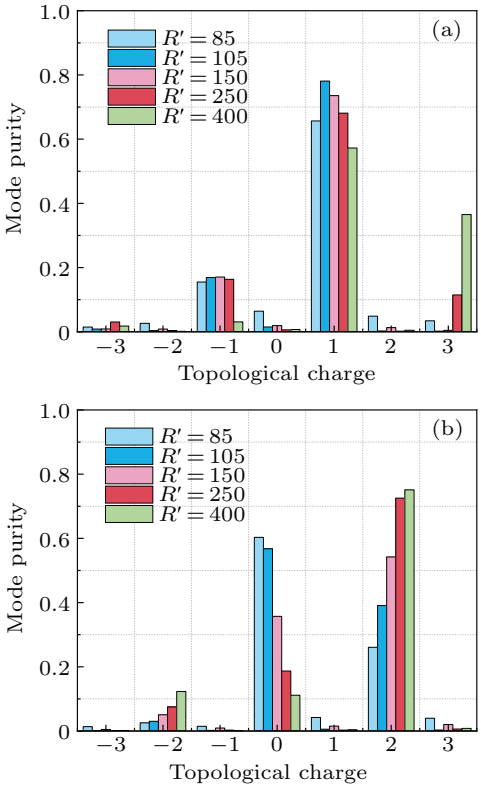


Fig. 4. OAM spectra of vortex electromagnetic wave with $l = 1$ (a) and $l = 2$ (b) after passing keyholes with different radii of target trajectory.

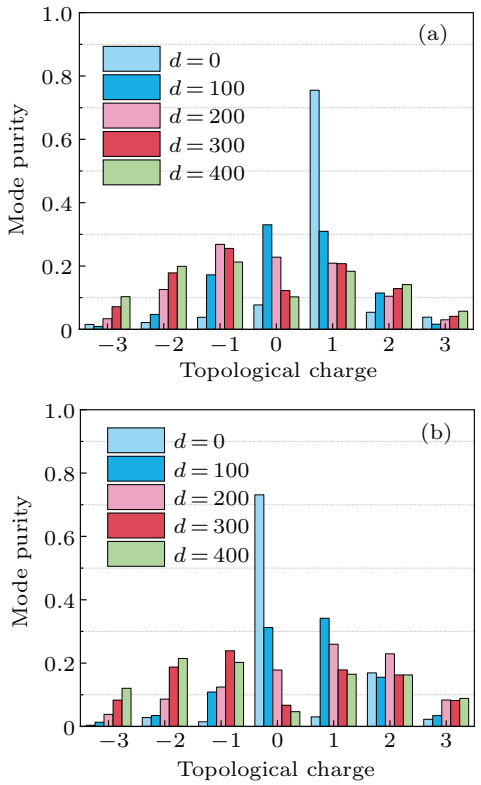


Fig. 5. OAM spectra of vortex electromagnetic wave with $l = 1$ (a) and $l = 2$ (b) after passing through keyhole when target is off-axis.

Figures 5(a) and 5(b) show the mode purities of OAM

beam with $l = 1$ and $l = 2$, respectively, when the target is off-axis. In the cases with $l = 1$ and $l = 2$, the OAM spectra spread both obviously, consequently, purities of their adjacent modes increase. On the one hand, the purity of main mode decreases gradually with $l = 1$ as the d increases from 0 mm to 400 mm, because the trajectory of the target moves away from the ring of the OAM beam gradually. On the other hand, for the case with $l = 2$, the target does not rotate at the ring when $d = 0$ due to the larger range of the hollow region and moves then far away from the ring when d exceeds 200 mm. Therefore, the purity of main mode $l = 2$ is improved when d increases from 0 to 200 mm and then decreases when d increases from 200 mm to 400 mm.

3.2. Measurement errors and analysis

In this subsection, the detection errors of a target that moves along the observation surface with a longitudinal acceleration and an angular acceleration in four situations are investigated by using composite OAM beam with $l = \pm 1$ and $l = \pm 2$. We consider the OAM modes with topological charge of $l = \pm 1$ and $l = \pm 2$ for the following reasons. Firstly, the OAM spectrum is dependent on the geometrical relation among the radiation region of vortex electromagnetic wave, the keyhole and the target. For higher-order OAM modes, the variation trend of OAM spectrum will not change. Secondly, it can be easier to generate lower-order vortex electromagnetic waves with high quality at the radio frequency. Meanwhile, the using of OAM modes with opposite topological charges makes it easy to analyze the OAM spectrum and investigate the detection errors. For the uniform acceleration case, the LUA and AUA are set as $g = 15$ m/s^2 and $g' = 100\pi$ rad/s^2, respectively, with initial velocity of $v_0 = 0$ and $\Omega_0 = 0$. For the variable acceleration case, the LVA and AVA are $p = 30$ and $p' = 300$ (m/s^3), respectively, with $g_0 = 0$ and $g'_0 = 0$.

Firstly, figures 6(a) and 6(b) show the detection errors for the cases that the different radii of keyhole with $l = \pm 1$ and $l = \pm 2$, respectively. As shown in Fig. 6(a), the detection errors of the AUA and the AVA with different radii of keyhole keep the same as those without keyhole existing, for the energy of the OAM beam with $l = 1$ and $l = -1$ illuminate the rotating target completely. The detection errors of AUA are all below 5%, while the detection errors of AVA keep below 15% with $l = \pm 1$. Meanwhile, all the detection errors of LUA and LVA remain below 1%. Figure 6(b) shows the detection errors for the $l = 2$ and $l = -2$. It is known that the higher mode will bring larger rotational Doppler shift, resulting in the lower detection errors of AUA and AVA. As a result, the detection errors of angular accelerations can be reduced by using higher modes when the radius of keyhole is larger. It can be seen that the errors of the AUA decrease from 100.4% to 1.3% and the errors of AVA fall from 80.4% to 3.78% gradually. It can be well explained by the fact that when the aperture is small, most of the energy of the higher-order mode is reflected back, and only a small potion of radiation irradiates the target, thus causing purity of mode to diverge into the value in the case $l = 0$. Then the purity of main mode is increased obviously as the aperture size turns larger. When the aperture size is infinite, it is equivalent to the transmission of vortex electromagnetic wave in free space, and the higher the order of OAM mode used for detection, the smaller the errors of angular acceleration is.[12] Therefore, for angular accelerations, we should select the maximum OAM mode so that the detection errors can be reduced through using the aperture. However, the errors of LUA and LVA do not change linearly. According to Eq. (3), the detection of LUA and LVA are affected by not only the slope m, but also the detection values of AUA and AVA. In fact, we can emit a spherical wave with $l = 0$ to eliminate the influence of obstacles on the vortex electromagnetic wave spectrum spreading, which are discussed in the following cases.

Secondly, figures 6(c) and 6(d) show the detection errors for the different thickness of keyhole with $l = \pm 1$ and $l = \pm 2$, respectively. It can be found that the distribution of OAM spectrum is similar to those of different aperture sizes in Figs. 2 and 3. Therefore, the changing trends of errors are the same in two cases. Due to the small range of energy with $l = \pm 1$, the purities of main modes are almost unaffected when passing through keyholes with different thickness. As shown in Fig. 6(c), the detection errors of AUA are below 5%, those of AVA keep below 15%, and those of LUA and LVA are below 1.5%. Figure 6(d) shows the plots of the detection errors for $l = 2$ and $l = -2$, the errors of AUA are decrease from 89.325% to 1.25% and the errors of AVA fall from 72.48% to 5.45% apparently as the thickness of keyhole increases. It can be seen in Fig. 3(b) that the larger aperture thickness limits the divergence of the higher-order modes and improves the purity of the main mode with $l = 2$. Therefore, the errors of angular accelerations decrease gradually. Interestingly, it is noted that the detection errors increase a little when $w = 200$ mm compared with when $w = 100$ mm. It is because the higher modes can bring larger Doppler frequency shifts, which indicates whether the frequency shift fitting exceeds the display range in the time–frequency diagrams should be considered when the purities of higher modes increase to a certain value. It can be reduced by increasing the sampling time or adding a deblurring function before signal processing.

Thirdly, figures 6(e) and 6(f) show the detection errors for the cases that the different radii of target trajectories with $l = \pm 1$ and $l = \pm 2$, respectively. For detecting the target accelerations, the detection errors can be minimized only when the target is illuminated by the main radiation region of the vortex electromagnetic wave. It can be seen in Fig. 6(e) that

the errors of AUA increase from 4% to 89.4% and the errors of AVA are raised from 13.17% to 106.49% with $l = \pm 1$. Meanwhile, the errors of LUA and LVA remain above 20% when $R' = 400$ mm. It can be explained that when the target moves outside the main radiation region of OAM beam, the purity of main mode spreads significantly to higher-order modes. As shown in Fig. 4(a), the purity of $l = 1$ is lowest and the purities of the high-order modes such as $l = 3$ increase obviously when $R' = 400$ mm. According to Eq. (5), the higher-order modes have a strong influence on the slope estimation, which causes the estimated value of m_1 to increase. Therefore, the detection errors increase apparently when $R' = 400$ mm with $l = \pm 1$. Figure 6(f) shows the plots of the errors for the case of $l = \pm 2$. It can be seen that the errors of AUA decrease to 1.625% and those of AVA fall to 7.2% due to the fact that the purities of main modes increase as the value of R' rises. Therefore, for different radii of target trajectory, we should comprehensively consider the radiation region of the vortex electromagnetic wave and the size of the aperture, then choose the appropriate OAM mode, so that the target can be illuminated by the energy of the vortex electromagnetic wave as much as possible, which can reduce the diffusion of main OAM purity.

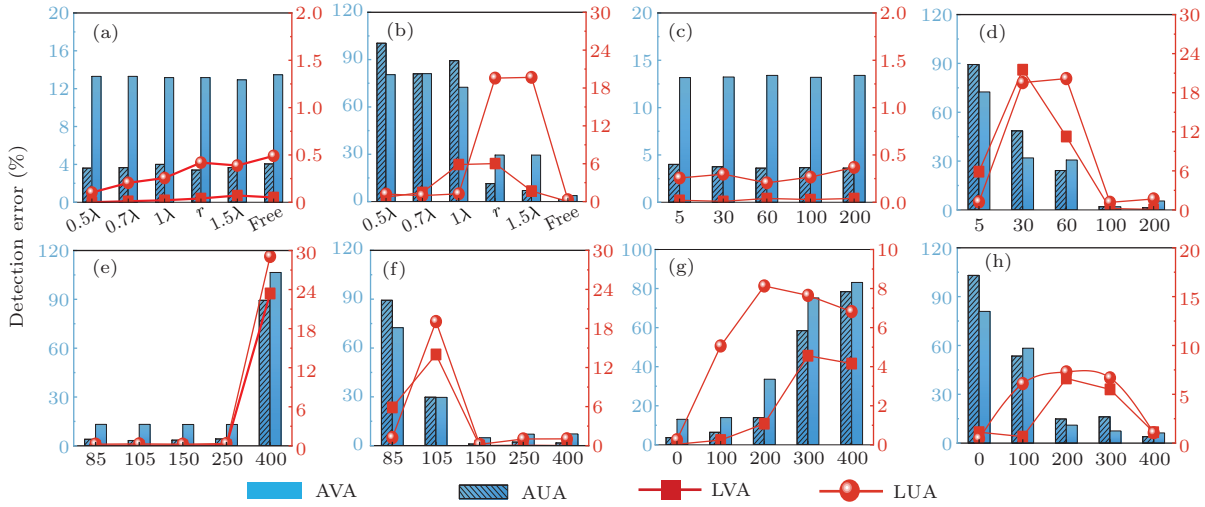


Fig. 6. Errors of uniform and variable accelerations, caused by difference among keyhole radii with $l = \pm 1$ (a) and $l \pm 2$ (b), difference among keyhole thickness with $l = \pm 1$ (c) and $l = \pm 2$ (d), difference among radii of target trajectories with $l = \pm 1$ (e) and $l = \pm 2$ (f), and difference among offset positions of target with $l = \pm 1$ (g) and $l = \pm 2$ (h).

Finally, figures 6(g) and 6(h) show the detection errors for the cases that the different off-axis positions of the target with $l = \pm 1$ and $l = \pm 2$, respectively. It is shown that the OAM spreading is obvious with $l = 1$ for the case that position of the target is off-axis due to only part of the trajectory is illuminated by the main radiation region of the OAM beam. As a result, figure 6(g) shows that the detection errors of AUA increase from 3.65% to 78.4% and those of AVA rise from 13.03% to 83.13% apparently with $l = \pm 1$. Meanwhile, the errors of LUA and LVA reach 5% as d rises. Figure 6(h) shows the detection errors for the cases of $l = \pm 2$. It is worth noting that the detection errors of AUA and AVA decrease to 3.9% and 6.23%, respectively, even though the OAM spectrum spreading is also obvious when $d = 200$ mm, 300 mm, and 400 mm. According to Eq. (5), $l = 3$ and $l = 1$ may have opposite effects on the slope estimation with $l = 2$. Therefore, errors in the detection of angular accelerations may be rather lower with $l = \pm 2$. To demonstrate it, figure 7 shows the time–frequency diagrams of $d = 400$ mm with $l = \pm 2$. As shown before, there are many interference items in Figs. 7(a) and 7(b), but the errors of accelerations are rather small in Fig. 6(h).

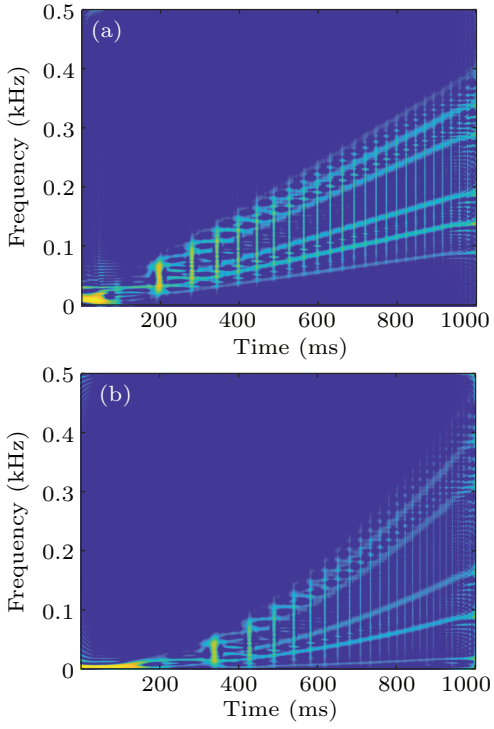


Fig. 7. Time–frequency diagrams of echo signal of (a) uniformly and (b) variably accelerated target with $l = \pm 2$ when $d = 400$ mm is detected.

In order to consider the practicability of the results, we

change the value of signal-to-noise ratio (SNR) to 15 dB. Without loss of generality, the cases of different radii of keyhole are studied, and the detection errors are calculated. As shown in Fig. 8, the changing trends of detection errors are stable at an SNR of 15 dB in comparison with the results in Figs. 6(a) and 6(b).

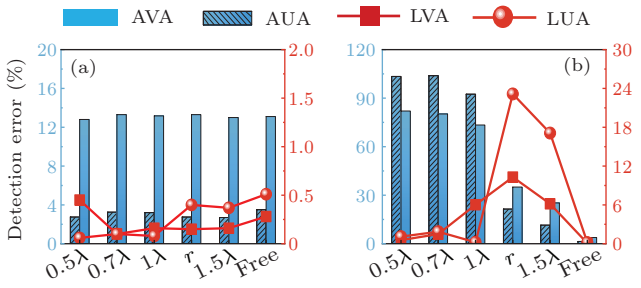


Fig. 8. Errors of uniform and variable accelerations at signal-to-noise ratio of 15 dB, caused by difference among radii of keyhole with $l = \pm 1$ (a) and $l = \pm 2$ (b).

According to the above analysis, the discrete time–frequency signal leads to the detection errors of the target accelerations, which are caused by the spread of the OAM spectrum when OAM beam does not completely illuminate the rotating object. In fact, the detection ability of the OAM beam is determined by the relative position among the main radiation region of the vortex electromagnetic wave, the keyhole and rotating object. When the selected OAM mode is not blocked by the keyhole and the rotating object moves in its main radiation region, the detection errors of the target accelerations are minimized. Therefore, by pre-measuring the amplitudes of OAM beams with different modes transmitted by the antenna and by comparing with the aperture size and the attitude of the target, then the reasonable selection of the OAM modes, which are less affected by keyhole and illuminate the trajectory of the detected target as much as possible, can effectively reduce the error of angular acceleration, because the error is directly affected by the purities of main OAM modes. For example, when the size of the aperture or the trajectory of the target is large, we need to use higher-order modes to obtain higher OAM purities and thus smaller angular acceleration errors are obtained. Instead, smaller OAM modes should be used to ensure the accuracy of the detection. For the longitudinal acceleration of the target, we can emit vortex electromagnetic wave with l =0 to detect target and eliminate the influence of OAM spectrum, from which the obtained conclusion is obviously different from the conclusion that the detection accuracy by using high-order OAM modes is higher than that of low-order OAM modes when the target accelerations are detected in free space.[12]

In particular, we consider a special case that the acceleration is set to 0. According to Eq. (2), when $g = 0$ and $g' = 0$, the Doppler shift formula can be expressed as

$$\Delta f(t) = \frac{1}{2\pi} \cdot \frac{\mathrm{d}\Delta\varphi(t)}{\mathrm{d}t} = \frac{2f_c v_0}{c} + \frac{l\Omega_0}{2\pi}. \tag{9}$$

The longitudinal velocity and the angular velocity are set as $v_0 = 1.5$ m/s and $\Omega_0 = 40\pi$ rad/s, respectively.

For example, the OAM spectral spreading of $R = 0.5\lambda$ with $l = 1$ in Fig. 2(a) is chosen. When the fast Fourier transform (FFT) is performed on the echo signal with respect to t, the frequency spectrum is shown in Fig. 8. It is found that the angular velocity and longitudinal velocity can be calculated by transmitting a single OAM mode. The angular velocity can be accurately calculated by using the frequency shift difference (20 Hz) between adjacent modes, and the longitudinal velocity can be calculated by frequency shift (24.5 Hz) of the component of $l = 0$ in simulation.[36]

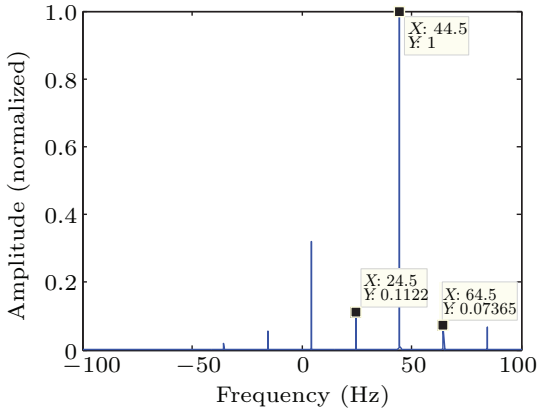


Fig. 9. Simulation frequency spectrum of the echo when $v_0 = 1.5$ m/s and $\Omega_0 = 40\pi$ rad/s.

Finally, it is necessary to point out that spectral components may be missing in the experiment.[37] To reduce the errors, the minimum frequency shift difference should be used to estimate the angular velocity.

4. Conclusions

In conclusion, this work studies the errors in detection of accelerations in keyhole space. Based on the effect of OAM spectrum spreading which is simulated and analyzed, the errors of accelerations of uniformly and variably accelerated targets in keyhole space under different composite OAM beams are calculated and compared by the multi-mode method. The results show that the errors can be reduced effectively by using a combination of appropriate modes in different cases. The change in keyhole and attitude of the target will embody in the relativeness between radiation region of vortex electromagnetic wave and the attitude of receiving surface.

Acknowledgement

Project supported by the National Natural Science Foundation of China (Grant Nos. 11804073 and 61775050).

References

[1] Mohammadi S M, Daldorff L K S, Bergman J E S, Karlsson R L, Thide B, Forozesh K, Carozzi T D and Isham B 2009 *IEEE Trans. Antennas Propag.* **58** 565

[2] Edfors O and Johansson A J 2012 *IEEE Trans. Antennas Propag.* **60** 1126

[3] Allen L, Beijersbergen M W, Spreeuw R J C and Woerdman J P 1992 *Phys. Rev. A.* **45** 8185

[4] Chen R, Xu H, Moretti M and Li J D 2018 *IEEE Wireless. Commun. Lett.* **7** 582

[5] Lei Y, Yang Y, Wang Y Z, Guo K, Gong Y B and Guo Z Y 2021 *IEEE Wireless. Commun. Lett.* **10** 261

[6] Wang Y L, Wang Y Z and Guo Z Y 2022 *Measurement* **189** 110600

[7] Liu D, Shi H Y, Liu H, Yang T and Guo J W 2023 *IEEE Sens. J.* **23** 8478

[8] Liu K, Cheng Y Q, Yang Z C, Wang H Q, Qin Y L and Li X 2014 *IEEE Antennas Wireless Propag. Lett.* **14** 711

[9] Bu L, Zhu Y, Chen Y, Song X O, Yang Y F and Zang Y D 2022 *Remote. Sens-Basel* **14** 5908

[10] Zhao M Y, Gao X L, Xie M T, Zhai W S, Xu W J, Huang S G and Gu W Y 2016 *Opt. Lett.* **41** 2549

[11] Zhou Z L, Cheng Y Q, Liu K and Liu H Y 2018 *IEEE International Conference on Microwave and Millimeter Wave Technology (ICMMT)*

[12] Wang Y Z, Wang Y L, Guo K and Guo Z Y 2022 *Measurement* **187** 110278

[13] Xu P, Liu H X, Li L, Zhang K Y and Li L 2022 *IEEE Trans. Antennas Propag.* **70** 10678

[14] Xu P, Li L, Li R J and Liu H X 2022 *IEEE Trans. Antennas Propag.* **69** 7041

[15] Xie M T, Guo X L, Zhao M Y, Zhai W S, Xu W J, Qian J W, Lei M Z and Huang S G 2017 *IEEE Antennas Wireless Propag. Lett.* **16** 1143

[16] Yao Y, Liang X L, Zhu M H, Zhu W R, Geng J P and Jin R H 2019 *IEEE Trans. Antennas Propag.* **67** 2085

[17] Torner L, Torres J P and Carrasco S 2005 *Opt. Express* **13** 873

[18] Ren Y X, Huang H, Xie G D, *et al.* 2013 *Opt. Lett.* **38** 4062

[19] Wang H Y, Yang Z H, Liu L, Chen Y H, Wang F and Cai Y J 2023 *Opt. Express* **31** 916

[20] Cheng M J, Guo L X, Li J T, Huang Q Q, Cheng Q and Zhang D 2016 *Appl. Opt.* **55** 4642

[21] Hu Y Y, Zhang M, Dou J T, Zhao J and Li B 2022 *Opt. Express* **30** 42772

[22] Mitri F G 2011 *IEEE Trans. Antennas Propag.* **59** 4375

[23] Liu K, Liu H Y, Wei E. I. Sha, Cheng Y Q and Wang H Q 2020 *IEEE Antennas Wireless Propag. Lett.* **19** 1167

[24] Sun M H, Liu S H, Guo L X, Huang K and Cheng M J 2023 *J. Appl. Phys.* **133** 124905

[25] Liu K, Li X, Gao Y, Wang H Q and Cheng Y Q 2017 *J. Appl. Phys.* **122** 124903

[26] Gong T, Cheng Y Q, Li X and Chen D C 2018 *IEEE Microw. Wirel. Co.* **28** 843

[27] Zheng J Y, Zheng S L, Shao Z L and Zhang X M 2018 *J. Appl. Phys.* **124** 164907

[28] Zhou Z L, Cheng Y Q, Liu K, Wang H Q and Qin Y L 2019 *IEEE Sens. Lett.* **3** 2475

[29] Liu B Y, Henry Giddens, Li Y, He Y J, Wong S W and Hao Y 2020 *Opt. Express* **28** 3745

[30] Wang Y, Liu K, Liu H Y, Wang J Q and Cheng Y Q 2021 *IEEE Sens. J.* **21** 4989

[31] Chizhik D, Foschini G J, Gans M J and Valenzuela R A 2002 *IEEE Trans. Wireless. Commun.* **1** 361

[32] Almers P, Tufvesson F and Andreas Molisch F 2003 *IEEE Trans. Wireless. Commun.* **5** 3596

[33] Chen R, Xu H, Wang X D and Li J D 2018 *IEEE Wireless. Commun. Lett.* **8** 313

[34] Das D, Bora P K and Bhattacharjee R 2018 *IEEE Commun. Lett.* **22** 1834

[35] Yang Y, Gong Y B, Guo K, Shen F, Sun J H and Guo Z Y 2020 *IEEE Access* **8** 53232

[36] Gong T, Cheng Y Q, Li X and Chen D C 2018 *IEEE Microw. Wirel Technol.* **28** 843

[37] Qiu S, Ding Y, Liu T, Liu Z L and Ren Y 2022 *Opt. Express* **30** 20441